Icarus **158**, 42–55 (2002)
doi:10.1006/icar.2002.6874

Spectroscopy of Loose and Cemented Sulfate-Bearing Soils: Implications for Duricrust on Mars

Christopher D. Cooper and John F. Mustard

Department of Geological Sciences, Box 1846, Brown University, Providence, Rhode Island 02912
E-mail: Christopher_Cooper@brown.edu

Received September 7, 2000; revised December 17, 2001

The goal of this work is to determine the spectroscopic properties of sulfate in martian soil analogs over the wavelength range 0.3 to 25 μm (which is relevant to existing and planned remotely sensed data sets for Mars). Sulfate is an abundant component of martian soil (up to 9% SO_3 by weight) and apparently exists as a particulate in the soil but also as a cement. Although previous studies have addressed the spectroscopic identity of sulfates on Mars, none have used laboratory mixtures of materials with sulfates at the abundances measured by landed spacecraft, nor have any works considered the effect of salt-cementation on spectral properties of soil materials. For this work we created mixtures of a palagonitic soil (JSC Mars-1) and sulfates ($MgSO_4$ and $CaSO_4 \cdot 2H_2O$). The effects of cementation were determined and separated from the effects of packing and hydration by measuring the samples as loose powders, packed powders, cemented materials, and disaggregated materials. The results show that the presence of particulate sulfate is best observed in the 4–5 μm region. Soils cemented with sulfate exhibit a pronounced restrahlen band between 8 and 9 μm as well as well-defined absorptions in the 4–5 μm region. Cementation effects are distinct from packing effects and disaggregation of cemented samples rapidly diminishes the strength of the restrahlen bands. The results of this study show that sulfate in loose materials is more detectable in the near infrared (4–5 μm) than in the thermal infrared (8–9 μm). However, cemented materials are easily distinguished from loose mixtures in the thermal infrared because of the high values of their absorption coefficient in this region. Together these results suggest that both wavelength regions are important for determining the spatial extent and physical form of sulfates on the surface of Mars.

Key Words: **Mars' surface; spectroscopy; mineralogy.**

INTRODUCTION

The Viking and Mars Pathfinder landers measured the elemental chemistry of martian soil materials (Table I) and detected significant amounts of sulfur in the range of 5–10% by weight SO_3 (Toulmin *et al.* 1977, Clark *et al.* 1982, Rieder *et al.* 1997). The sulfur is thought to be in the form of sulfate due to the strongly oxidizing nature of the surface (Toulmin *et al.* 1977). The abundance of sulfate varies in different materials found at the landing sites, with crusts and clods at the Viking sites generally containing more sulfate than loose, powder materials (Baird *et al.* 1977, Clark *et al.* 1982, Clark 1993). The association of more cohesive materials with higher levels of sulfur, chlorine, and magnesium abundances (Clark 1993) supports a hypothesis that crusts and clods are soils that have been cemented by sulfate salts, likely $MgSO_4$ (Toulmin *et al.* 1977, Clark and Hart 1981). Further support for a salt-cementation process is the relationship between some crusts and local rocks. Some of the crusts appear to cling to rocks (Fig. 1), suggesting that the material had been cemented in place onto the surface of the rocks (Binder *et al.* 1977, Mustard 1997).

The APXS instrument on the Sojourner rover also measured compositions of rocks near the Mars Pathfinder landing site and found that they were chemically different from the soils (Rieder *et al.* 1997). The differences in chemical composition between rocks and soils as well as the existence of cemented materials at the Viking sites suggest that significant amounts of processing was needed to form the soils on Mars. Soils appear to be mixtures of locally derived lithic fragments, a globally homogeneous dust that is likely weathered basalt, and a sulfate and chloride salt component (McSween and Keil 2000). Cementation of soils by sulfate salts in particular points to a likely role of water in the formation or alteration of much of the surface materials on Mars. The exact nature of this pedogenic process and the role that water plays is uncertain however. Understanding the mineralogical nature and abundance of sulfate salts could provide insight into the processes that cemented the surface materials and the environmental conditions at the time of formation. A number of models have been proposed to explain the origin of sulfate salts, including evaporation of bodies of water (Burns 1993, Schaefer 1993, Catling 1999), atmosphere–surface interactions including volcanic aerosols and acid-fog weathering (Clark and Baird 1979, Settle 1979, Clark and Hart 1981, Banin *et al.* 1993, 1997), and hydrothermal alteration (Allen *et al.* 1981, Bell *et al.* 1993, Griffith and Shock 1997, Newsom *et al.* 1999). Theoretical and experimental studies of the interactions of rocks and water under martian conditions also have been performed to understand the origin of salts (Schaefer 1993, Moore and Bullock 1999).

0019-1035/02 $35.00

TABLE I
Compositions of Martian Surface Materials

Oxide	VL-1 fines	VL-2 fines	MPF drift	VL-1 clods	MPF crust
SiO_2	43	43	47.9	42	51.6
Al_2O_3	7	7.3	8.7	7	9.1
TiO_2	0.66	0.56	0.9	0.59	1.1
Fe_2O_3	18.5	17.8	17.3	17.6	13.4
CaO	5.9	5.7	6.5	5.5	7.3
MgO	6	6	7.5	7	7.1
K_2O	<0.15	<0.15	0.3	<0.15	0.5
SO_3	6.6	8.1	5.6	9.2	5.3
Total	88.5	89.1	98	89.7	98

Note. Viking compositions from Clark *et al.* (1982); Pathfinder compositions from Rieder *et al.* (1997) with FeO values instead of Fe_2O_3. Drift = A-5; Crust = A-8.

In order to better understand the formation of soil materials and to test various models of pedogenic processes, the mineralogy of the materials needs to be determined. The chief tool for determining mineral compositions for surface materials has been spectroscopy performed from orbit or telescopically. Visible to near-infrared spectroscopy has helped constrain the identity of the ferric iron component in the martian soils (Singer *et al.* 1979, Morris *et al.* 1989, Bell *et al.* 1990, 1993, 2000, Bishop *et al.* 1993, Morris *et al.* 1993, 2000, Murchie *et al.* 1993) and has identified the composition of some crustal materials including basalts containing two types of pyroxene (Mustard and Sunshine 1995). Recent thermal infrared observations by the Thermal Emission Spectrometer (TES) on the Mars Global Surveyor spacecraft have confirmed basaltic compositions (Christensen *et al.* 2000b) and also identify another component that may be less mafic surface materials (Bandfield *et al.* 2000). TES data have also identified regions of coarse-grained hematite (Christensen *et al.* 2000a).

Observations of soil mineralogy and sulfates in particular are much less certain. Previous workers have tentatively identified sulfates based on weak absorptions in telescopic data (Pollack *et al.* 1990, Blaney and McCord 1995). These spectra suffered from a number of factors that complicated their interpretation and made the detection of sulfates challenging. The thermal infrared spectra of Pollack and others (1990) required a theoretical atmospheric correction. The results suggested sulfate or bisulfate, but it was ambiguous as to whether the material existed in the atmosphere or on the surface. Blaney and McCord (1995) used spectra from the crossover region between reflected solar radiation and emitted thermal radiation (4–5 μm). Because atmospheric absorptions partially overlap with the proposed sulfate feature, uncertainties in modeling the atmosphere in the crossover region makes removal of the continuum as well as determination of band strengths and shapes difficult.

A further problem that affected both studies was the lack of good sulfate analog materials that could be compared spectroscopically to the observations of Mars. Spectra of pure, relatively coarse grained sulfates were used for comparison, though these materials are unlike what is expected for most surfaces on Mars. Other studies of sulfates have used finer fractions of powdered

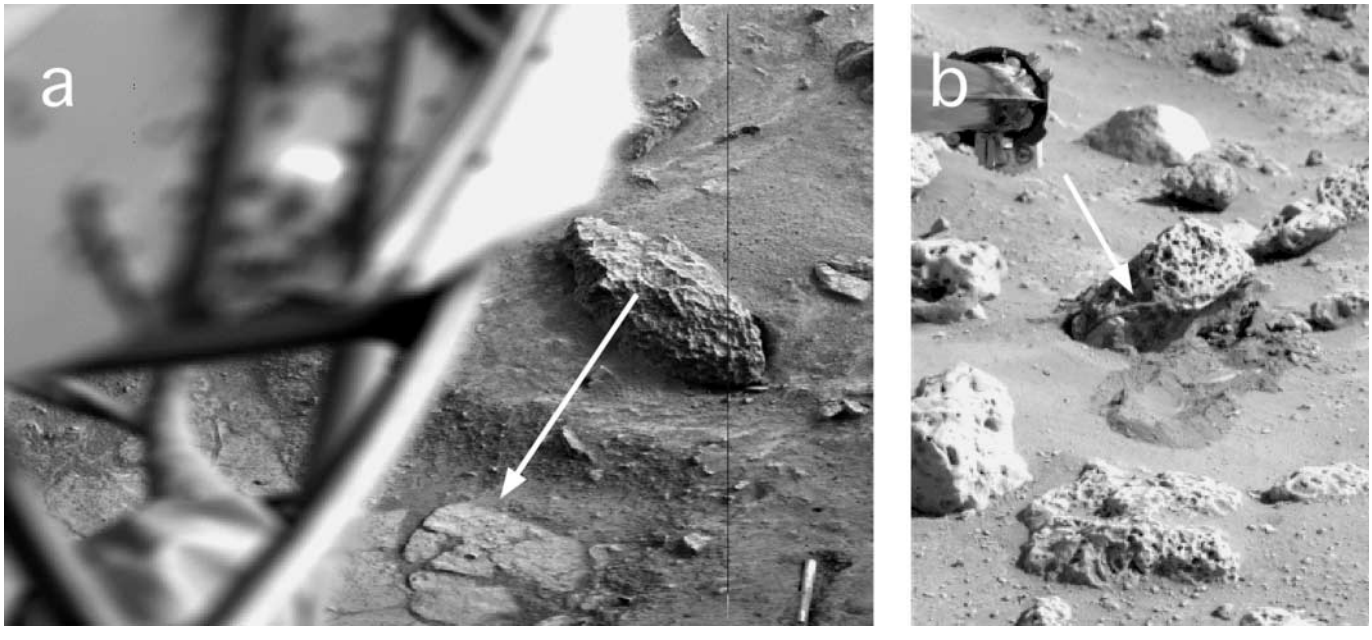

FIG. 1. Two images of cohesive materials observed by the Viking Landers and interpreted to be salt-cemented soils. (a) Blocky material uncovered by landing rocket exhaust at Mutch Memorial Station (VL1; Frame 12C158); (b) cohesive material adhering in a layer to a rock dislodged by the lander arm at VL2 (Frame 22B030).

material (Lane and Christensen 1998), but none have addressed the process of mixing and cementation with spectrally neutral materials. Additionally, these studies have concentrated on limited portions of the electromagnetic spectrum, with none addressing the full range from the visible to the thermal infrared. This work systematically examines the spectra of mixtures of sulfates and palagonites to understand the changes in spectra that occur with cementation in order to produce better analogs for comparison with observations of Mars. Observations are made across the entire wavelength range from 0.3 to 25 μm, which permits a better understanding of the cementation process and its effects on the interaction between the cohesive materials and electromagnetic radiation. The broad spectral range also makes this study applicable to the observations of a number of instruments, from TES to planned spectrometers on future orbiters including THEMIS and OMEGA. The increases in spatial resolution and data quality coupled with the insight into the behavior of cemented materials provided by this study should allow the mapping of sulfate content and the distribution of cemented soils on Mars.

TABLE II
Compositions of Experimental Mixtures

	Wt% $MgSO_4$ mixed with JSC Mars-1[a]						Wt% $CaSO_4 \cdot 2H_2O$ added	
Oxide	0	5.1	7.6	10.0	12.4	18.1	12.4	23.8
SiO_2	43.5	41.3	40.3	39.2	38.1	35.7	38.1	33.1
Al_2O_3	23.3	22.1	21.6	21.0	20.4	19.1	20.4	17.8
TiO_2	3.8	3.6	3.5	3.4	3.3	3.1	3.3	2.9
Fe_2O_3	15.6	14.8	14.4	14.0	13.7	12.8	13.7	11.9
MnO	0.3	0.3	0.3	0.3	0.3	0.3	0.3	0.2
CaO	6.2	5.9	5.7	5.6	5.4	5.1	8.3	10.3
MgO	3.4	4.9	5.6	6.4	7.1	8.8	3.0	2.6
K_2O	0.6	0.6	0.6	0.5	0.5	0.5	0.5	0.5
Na_2O	2.4	2.3	2.2	2.2	2.1	2.0	2.1	1.8
P_2O_5	0.9	0.9	0.8	0.8	0.8	0.7	0.8	0.7
SO_3	—	3.4	4.9	6.6	8.2	11.9	5.8	11.1
Total	100	100	100	100	100	100	96.3	92.8

[a] JSC Mars-1 after removal of water from Allen *et al.* (1998).

EXPERIMENTAL APPROACH

We created a number of experimental materials to investigate the effects of sulfate type, concentration, and the salt-cementation process on the remotely sensed signatures of martian analogs. Mixtures of a palagonitic soil and two types of sulfate were created and examined systematically to understand separately the spectral differences caused by (a) variations in sulfate abundance, (b) textural differences resulting from packing, cementation, and disaggregation, and (c) the hydration state of the sulfate minerals.

For the mixtures we used JSC Mars-1 palagonite as a spectrally neutral base material that matches well with the silicate and oxide portions of the martian soil. This palagonite is a well-characterized altered volcanic tephra from Mauna Kea, Hawaii, that is widely used as an analog for the martian soil and is freely available to researchers (Allen *et al.* 1998). The two sulfates used were anhydrous magnesium sulfate ($MgSO_4$) and gypsum ($CaSO_4 \cdot 2H_2O$), both of which were reagent grade materials. In the remainder of this paper the gypsum will be referred to as $CaSO_4$, but mass fractions are calculated correctly including the structural water.

Particle size plays an important role in controlling the spectral characteristics of powders (e.g., Salisbury and Eastes 1985, Crown and Pieters 1987, Salisbury and Wald 1992, Clark 1999) and in particular very fine particle sizes have unique spectral effects (Mustard and Hays 1997, Cooper and Mustard 1999). Therefore care was taken to match the physical properties of the martian surface materials, especially a particle size of less than 15 μm (Moore *et al.* 1987, 1999, Erard *et al.* 1994, Pollack *et al.* 1995, Ferguson *et al.* 1999, Tomasko *et al.* 1999). Both the palagonite and the sulfates were sieved to <15 μm before mixing, and the mixtures were then lightly ground with a mortar and pestle to ensure that the two materials were uniformly distributed.

Mixtures of both magnesium and calcium sulfates were made with the palagonite in proportions chosen to bracket the measured sulfur concentrations on Mars. The chemical compositions of the mixtures were calculated based on the published composition of JSC Mars-1 (Allen *et al.* 1998) and are listed in Table II. With sulfur expressed as percent SO_3 by weight, these mixtures bracket the compositions measured by the Viking and Pathfinder landers (Table I).

Sample texture is widely known to affect the spectral properties of materials (e.g., Lyon 1964, 1965, Hunt and Vincent 1968, Vincent and Hunt 1968, Adams 1975, Hapke 1983, Pieters 1983, Salisbury *et al.* 1991, Johnson *et al.* 1998). Thus the experiments were designed to span the range of textural factors other than particle size in order to isolate the effects of cementation from the others. Loose powders and cemented mixtures of each composition mixture were created, and disaggregated cemented mixtures and packed powders of a subset of the compositions were also made. Table III lists the textures for which spectra were gathered for each composition material. Powder samples were placed into stainless steel sample holders, lightly tapped to settle the powder, and leveled by scraping a straightedge across the surface at an angle to prevent compaction and to create a uniform surface texture (Mustard and Hays 1997). Packed powders were compressed into the sample containers using a flat stainless steel blade. Cementation was achieved by adding small amounts (<0.3 mL) of deionized water to $\sim$0.5 g of powder material to form a paste and packing the paste into a sample container. The container with the paste mixture was then dried for approximately 20 minutes in a 150°C oven. The exact times and temperatures were chosen to prevent efflorescence of the sulfate onto the surface of the sample, thus ensuring a homogeneous material for later measurements. Cemented samples

TABLE III
Measurement Conditions of Experimental Materials

Sample	Loose	Packed	Cemented	Disaggregated	Packed
$MgSO_4$					
0%	×	×	×	×	×
5.1%	×	×	×		
7.6%	×	×	×		
10.0%	×	×	×		
12.4%	×	×	×		
18.1%	×	×	[a]		
100%	×	×	×	×	×
$CaSO_4$					
0%	×	×	×	×	×
12.4%	×	×	×		
23.8%	×	×	×		
100%	×	×	×	×	×

[a] Used in microprobe analysis to match SO_3 concentration of 23.8% $CaSO_4$ sample. The material surface was too irregular for spectral measurements.

were also disaggregated by crushing and lightly grinding in a mortar and pestle and were sieved to the same particle size range as the initial powders (<15 μm).

The spectral reflectance properties of these preparations were measured from 0.3 to 25 μm using the RELAB facilities at Brown University (Pieters 1983; see also Mustard and Pieters 1989). The visible to near-infrared portion from 0.35 to 2.6 μm was measured using the bidirectional RELAB spectrometer at 5-nm spectral resolution, while the infrared portion from 0.9 to 25 μm was measured using a biconical Nicolet 740 Fourier transform infrared spectrometer (FTIR) with resolution of 4 cm^{-1}. For each sample the FTIR spectra were spliced and scaled to the radiometrically calibrated RELAB spectra. The splicing wavelengths were at 1.305 μm for $MgSO_4$ samples and 1.360 μm for $CaSO_4$ samples. The splice points were chosen to minimize noise and splice on a portion of the spectrum unaffected by absorption bands.

For powder samples of the particle size used here the biconical arrangement results in effectively diffuse scattering that produces spectra directly comparable to directional-hemispherical and emissivity measurements (Mustard and Hays 1997). However, for solid surfaces like the crusts, the biconical arrangement may result in spurious features in the restrahlen bands due to specular reflection (Salisbury *et al.* 1991). Specular reflections were eliminated from the biconical measurements of the cemented samples by measuring the samples in an off-axis geometry. In the normal biconical geometry, the light source, sample, and detector are coplanar. This leads to the measurement of specular reflections by the detector along with the diffusely reflected light that is of interest. In the off-axis geometry, the samples are placed in an accessory chamber where the incident beam is 90° to the direction at which the light is collected. This allows for a more accurate determination of the strength of the primary vibration features with high absorption coefficients and minimizes the distortion of the shape of these restrahlen bands. The splicing wavelength for samples measured in this off-axis geometry was 2.540 μm due to the different detector used for these measurements. Band strengths were calculated for sulfate bands by constructing a linear continuum across the band connecting the points of maximum reflectance on either side. The difference between the continuum and measured reflectances at the band center was then ratioed to the continuum reflectance (Clark and Roush 1984).

To assess in detail the grain-to-grain textural differences between calcium and magnesium cemented samples, thin sections were made and examined with an electron microprobe. The 18.1% $MgSO_4$ and 23.1% $CaSO_4$ cemented samples (both 12.0% SO_3) were vacuum impregnated with epoxy. These impregnated samples were then turned into thin sections, with denatured ethanol used for grinding and mineral oil used for polishing to prevent dissolution of the sulfate phases in the cemented samples. The thin sections were carbon coated and examined using the Brown University Cameca Camebax electron microprobe. Analysis was done with a 15-kV accelerating voltage and a 15-nA focused beam. Maps of electron backscatter were made along with elemental abundance maps of Ca, Mg, S, and Fe. These maps were used to analyze the physical relationships between the sulfate and palagonite phases of the cemented mixtures by correlating S and cation concentrations with grains visible in the backscatter maps.

RESULTS

Reflectance Spectra

Measuring reflectance spectra over the complete wavelength range from 0.3 to 25 μm enables characterization of sulfate mixtures in two important and complementary spectral regimes. These two regions, the visible to near infrared (0.3–5 μm) and the thermal mid-infrared (7–25 μm), each contain diagnostic sulfate absorptions (Fig. 2), yet have different optical properties

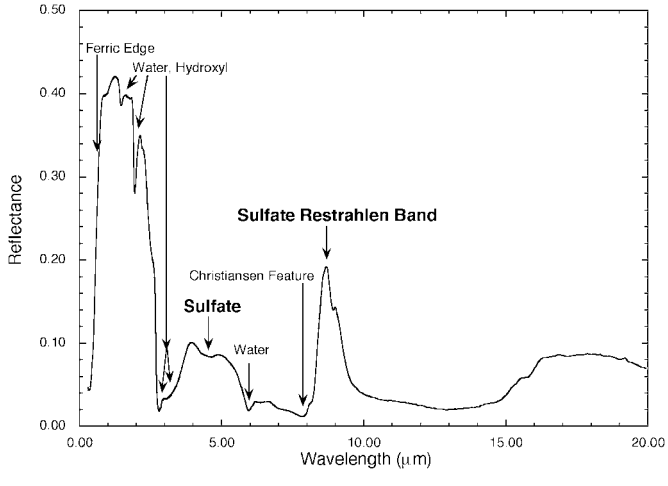

FIG. 2. The reflectance spectrum of a cemented mixture of JSC Mars-1 palagonite and 12.4% $MgSO_4$. Key spectral features are labeled.

and behaviors. The sulfate absorptions are the features near 4.5 and 9 μm that were tentatively identified in previous telescopic spectra of Mars as candidates for sulfate markers (Pollack *et al.* 1990, Blaney and McCord 1995).

The visible to near-infrared region up to 2.6 μm has absorption bands due to overtones and combinations of fundamentals of water, hydroxyl anions, and sulfate anions. The absorptions between 4 and 5 μm consist of overtones and combinations of overtones of bending and stretching vibrations of the sulfate anion (Salisbury *et al.* 1991). When water is present, the sulfate absorptions are likely modified by water vibrations. As a whole, the near-infrared region is characterized by low values of the absorption coefficient, k. This results in the dominance of volume scattering processes that are well understood and that involve regular behavior as a function of particle size (Moersch and Christensen 1995, Mustard and Hays 1997).

In the thermal infrared, k values are much more variable with values that range from amounts similar to the near-infrared regime to orders of magnitude higher. In particular, the k values are much higher at 8–9 μm, leading to sulfate restrahlen features from strong, mirrorlike first surface reflections (Moersch and Christensen 1995, Mustard and Hays 1997). This feature is due to the sulfate anion stretching fundamental (Salisbury *et al.* 1991). As particle sizes approach the wavelength of the light being reflected, very complex behavior is seen (Mustard and Hays 1997).

Figure 2 shows the locations of the both low-k sulfate absorptions between 4 and 5 μm and the reflectance peak of the restrahlen band due to a high-k sulfate absorption around 8.75 μm. This spectrum is of the cemented 12.4% $MgSO_4$ sample and is representative of the cemented mixtures. The spectrum also shows the ferric absorption edge ($\sim$0.5–0.8 μm) and the absorptions due to water (1.4, 1.9, 3, and 6 μm) and hydroxyl (1.4 and 2.2 μm). This paper concentrates on the sulfate features at 4–5 and 8.75 μm and examines their behavior as a function of sulfate abundance and textural preparation.

Loose powder sample spectra. Figure 3 shows the reflectance spectra of powder mixtures of the palagonite and sulfates. In Fig. 3a, the spectra of the suite of $MgSO_4$ mixtures display the range in band strengths that are seen in the 4–5 μm range. The sulfate absorptions there are sharp and well defined, and as expected they become stronger with increasing sulfate abundance in the mixture. The spectra of the loose powder mixtures of $CaSO_4$ (Fig. 3b) show similar reflectance properties in the near infrared although the overall suite of sulfate absorptions between 4 and 5 μm is less varied than observed in the $MgSO_4$ spectra. As seen in Fig. 4a, there is monotonic increase in band strength with the concentration of SO_3 for these absorptions. The relatively strong nature of the sulfate absorptions make the 4–5 μm range a good candidate for observing sulfates on Mars and will be covered by the OMEGA spectrometer.

In contrast, the thermal infrared portion of the spectra of both the magnesium and calcium sulfate powder mixtures is very bland. The only bands observed are due to volume scattering. The band depths for these absorptions are extremely weak ($<$0.2% for $MgSO_4$ and $<$2.0% for $CaSO_4$). The sulfate restrahlen band at 8.75 μm is not present, a result of the small particle size analogous to the behavior of silicates (Salisbury *et al.* 1991, Mustard and Hays 1997, Cooper and Mustard 1999). With a very high signal to noise ratio, the very subtle volume scattering bands might be observable. Their band strengths relative to the continuum are proportional to the amount of sulfate in the mixture as shown in Fig. 4b and in general are comparable to near-infrared band strengths. However, because these absorptions are extremely weak in terms of absolute band depth ($<$1–2%), they would be difficult to detect remotely.

Cemented sample spectra. While the behavior of the spectra of the loose powder samples was completely expected given the small particle sizes of the material ($<$15 μm), the spectra of the cemented materials (Fig. 5) are quite striking and somewhat surprising. The biggest difference between the spectra of cemented and loose $MgSO_4$ mixtures (Figs. 5a and 3a) is the extremely strong restrahlen band at 8.75 μm. This band is prominent for all of the cemented $MgSO_4$ mixtures, even at very low sulfate abundances. It is nearly as strong as the restrahlen band of the pure $MgSO_4$ cemented material. Pure $CaSO_4$ cemented material has a restrahlen band that is equal in strength to that of the pure $MgSO_4$ crust. In contrast, while each of the cemented $CaSO_4$ mixtures also has a restrahlen band, it is not nearly as strong as the band in the counterpart $MgSO_4$ mixtures. The spectra in Fig. 5b show that in the cemented mixtures, regardless of sulfate concentration, the $MgSO_4$ restrahlen band is stronger than the equivalent $CaSO_4$ mixture's restrahlen band.

There are additional changes in the thermal infrared beyond the restrahlen band. The continuum longward of $\sim$10 μm is higher in all of the cemented materials than in the loose powder materials. This is true even of the sulfate-free "cemented" palagonite sample that was prepared in an identical manner to that of the mixtures.

In contrast with the thermal infrared, the visible to near-infrared spectra of cemented materials are similar to their loose powder counterparts (compare Figs. 3 and 5). Overall reflectance is somewhat lower, but the water and hydroxyl bands are relatively unaffected (Fig. 6). The only major difference is in the $MgSO_4$ cemented samples in the 4–5 μm range. The sharp set of absorption bands seen in the loose powders has merged into a broad absorption similar to the $CaSO_4 \cdot 2H_2O$ band at the same position. This is likely due to combination overtones with water (Salisbury *et al.* 1991). The overall strength of the sulfate absorptions in this region changes little between the loose powder and cemented samples for either type of sulfate (Fig. 4a).

Textural issues. Because the process of making the cemented materials included pressing the moist paste into a dish before drying, the cemented samples are more compacted than the loose powder mixtures. To assess if compaction results in spectral properties similar to cementation, packed powder spectra of the sulfate mixtures were measured.

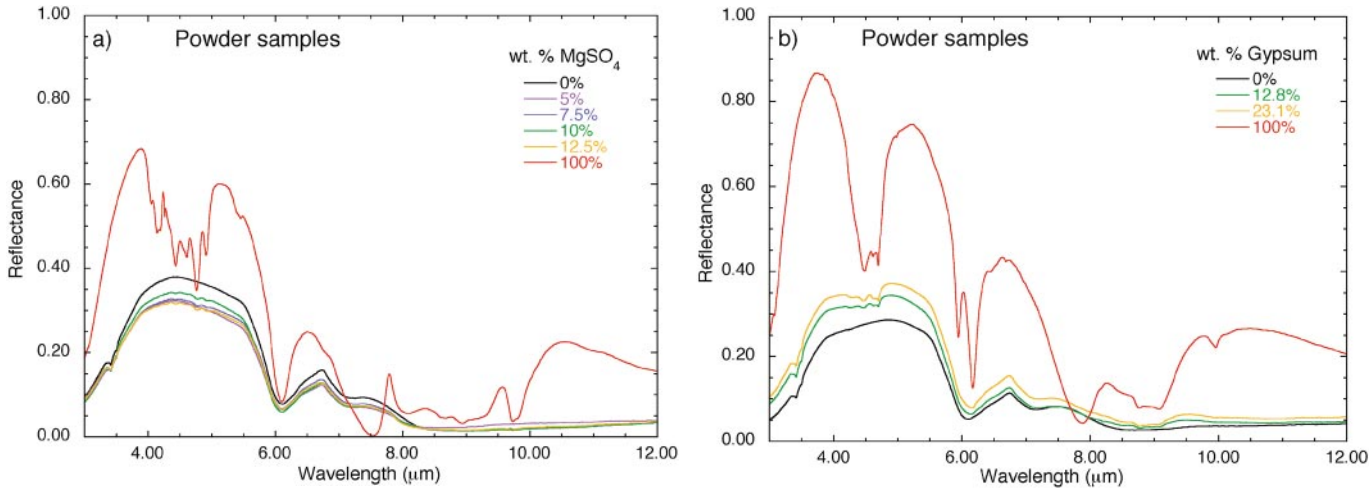

FIG. 3. Reflectance spectra of loose powder mixtures of palagonite and sulfate. Pure sulfate (heavy solid line) shows a wealth of diagnostic absorptions in the 4–5 μm range that are visible in the mixtures, while weaker features at ~9 μm are nearly indistinguishable in the mixtures. JSC Mars-1 palagonite mixed with (a) $MgSO_4$ and (b) gypsum ($CaSO_4 \cdot 2H_2O$).

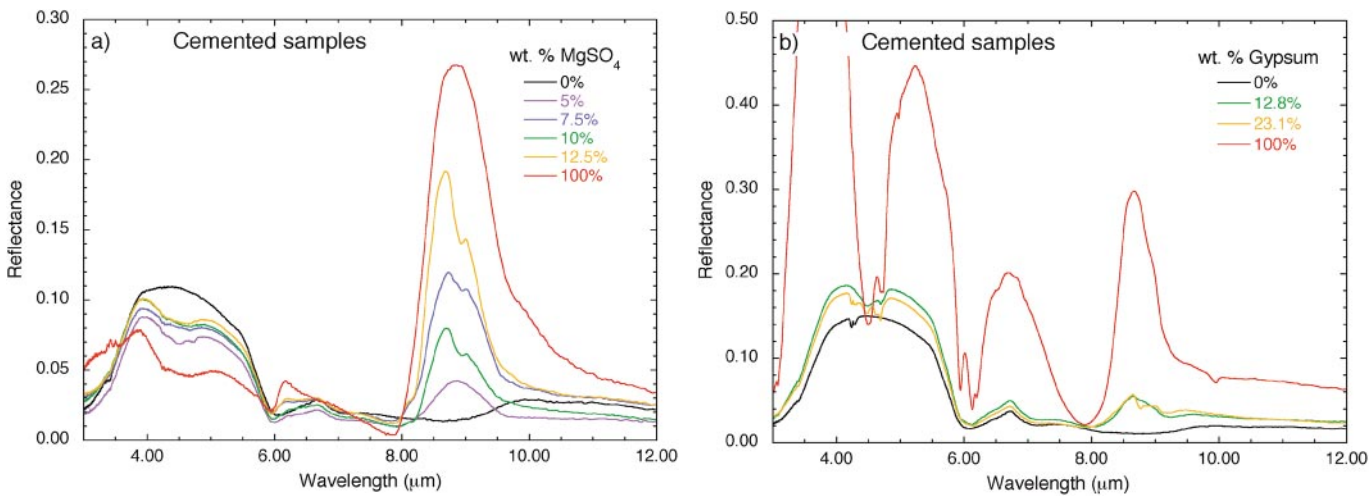

FIG. 5. Reflectance spectra of cemented mixtures of palagonite and sulfate. Compared to the powder mixtures in Fig. 2, the strength of the 4–5 μm absorptions remains relatively the same, while the restrahlen peak at 8.75 μm is much larger. $MgSO_4$ (a) shows stronger restrahlen peaks in mixtures than does $CaSO_4$ (b).

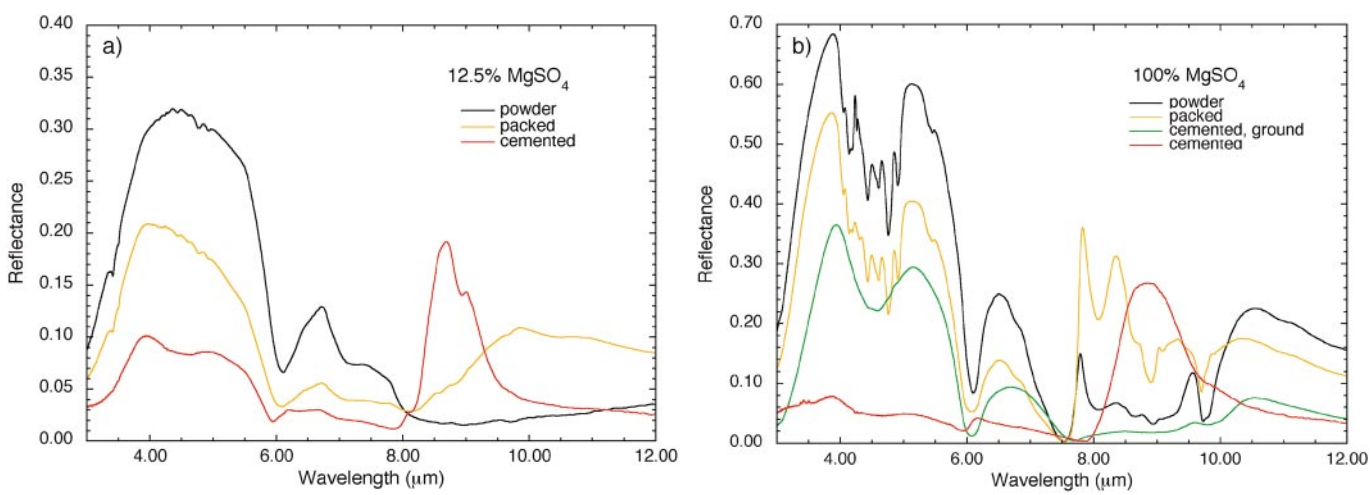

FIG. 7. Reflectance spectra of various textural preparations of (a) the 12.4% $MgSO_4$ mixture and (b) pure $MgSO_4$. In (a), the restrahlen peak at 8.75 μm is only visible in the cemented mixture and not in the packed powder, demonstrating that surface texture is not the principal control on the restrahlen band. Multiple restrahlen peaks reappear after heating at 260°C for 2 h, showing dependence of shape on hydration. In (b), the absorptions in the 4–5 μm region are sharp and distinct before adding water, while afterward they have merged into a single, broad absorption similar to that seen in the $CaSO_4$ mixtures (Fig. 2b). The restrahlen band, while different in shape and position, does not change in strength.

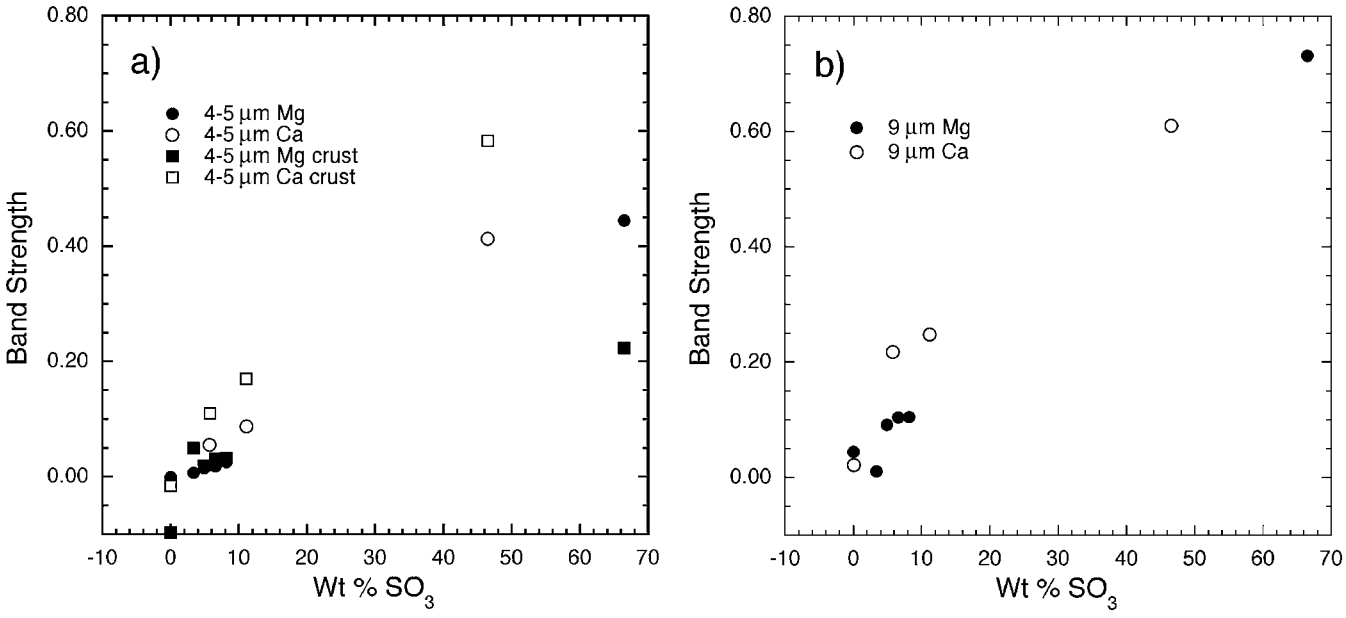

FIG. 4. Band strengths of the sulfate absorptions in the spectra of the powder mixtures shown in Fig. 3 (compositions are given in Table II). The sulfate absorptions are slightly stronger for calcium compared to magnesium. The 4–5 μm absorptions (a) have comparable strengths for loose and cemented preparations. The 4–5 μm absorptions are weaker than the 9-μm absorptions (b). However, the absolute band depths for the 9-μm absorptions are orders of magnitude lower than for the 4–5 μm absorptions.

Figure 7a shows the spectra of the 10% $MgSO_4$ mixture prepared as a loose powder, cemented, and as a packed powder. Figure 7b shows the spectra of the same preparations of the pure $MgSO_4$. Packing the mixtures produces a rise in the overall continuum longward of 10 μm matching that seen in the cemented mixtures. However, the 8.75-μm sulfate reflectance peak does not appear in the packed mixture, even though it is quite strong in the cemented mixture, suggesting that compaction does not cause the strength of the sulfate restrahlen peak. A second argument against simple compaction as the source of the strong 8.75-μm restrahlen bands in cemented $MgSO_4$–palagonite mixtures is that compaction would produce the same signal in similarly prepared $CaSO_4$ mixtures. The lack of a strong restrahlen band in these samples shows that another process is occurring in the cemented $MgSO_4$ mixtures that does not occur in the $CaSO_4$ counterparts to produce the strong restrahlen bands. Compaction of powdered samples does result in an increased reflectance of the continuum beyond 10 μm which is comparable to the increase in continuum reflectance observed in all cemented materials including the pure palagonite. This implies that the continuum reflectance is not a distinguishing feature of cementation.

Hydration of the $MgSO_4$. Another concern regarding the mixtures cemented with magnesium sulfate is the fact that the

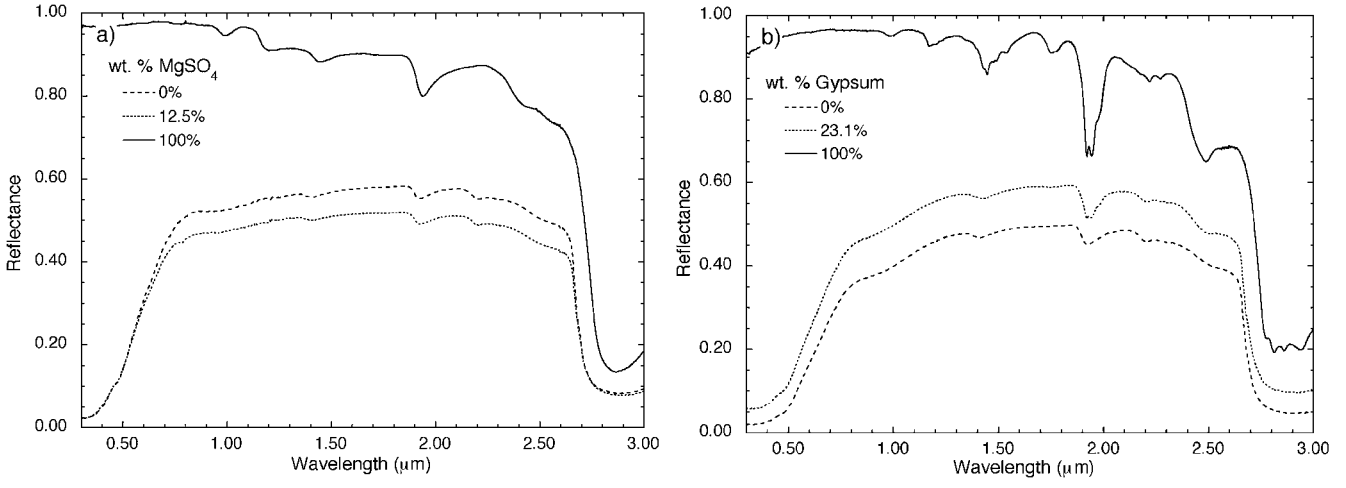

FIG. 6. Visible to near-infrared reflectance spectra of selected samples showing the lack of change in properties with addition of sulfate. Spectra are 0%, 12.4%, and 100% $MgSO_4$ materials as (a) powders and (b) cemented samples.

anhydrous sulfate becomes hydrated when water is added. This hydration of the sulfate phase could be expected to alter its spectral properties. To examine the effects of hydration on the $MgSO_4$ cemented mixtures, we disaggregated the pure $MgSO_4$ cemented sample and measured the resultant powder. We also packed this powder and measured it, and these measurements were compared to the same preparations of the anhydrous material.

Figure 7b shows the effects that hydration has on the spectra of $MgSO_4$. The loose powder $MgSO_4$ and the loose, disaggregated crust show the differences that occur with hydration in the 4–5 μm range. The broadening and merging of the separate, distinct sulfate absorptions in this range into a single absorption does appear to be due to hydration. This alteration in the spectrum is present in all textural preparations of the $MgSO_4$ after water has been added. The similarity of these spectra to those of the already water-bearing gypsum mixtures further strengthens this argument. It is likely that combinations and overtones of the water and sulfate vibrations are more numerous and less well defined than the anhydrous sulfate absorptions (Salisbury *et al.* 1991). This would lead to broader, less distinct absorption bands that would appear to create one broad, relatively smooth absorption. Additionally, the broadening and merging of the absorptions means that variations in the hydration state of the sample will introduce errors in the correlation of the 4–5 μm band strength with sulfate content. This affects the cemented magnesium sulfate samples in this study, with the 5.1% $MgSO_4$ appearing relatively dry compared to the other cemented $MgSO_4$ samples, explaining the higher than expected 4–5 μm band strength.

Hydration also affects the restrahlen band. In the packed powder $MgSO_4$ sample before hydration, two separated restrahlen peaks appear in contrast to the single peak observed in the cemented material and in the packed, hydrated powder. The separate peaks can be recovered in the cemented samples by heating (2 h at 260°C) to drive off the water (Fig. 7a), verifying that the changes in shape are due to hydration. The strength of reflection in the restrahlen region does not appear to change with hydration. So while hydration does affect the shape of the spectra in the thermal infrared, the strength of the restrahlen peak changes only very little and therefore would not affect the strength of the features seen in the cemented mixtures.

Microscopic Physical Relations between Sulfate and Palagonite

The above observations of the spectral properties of loose powders, packed powders, and cemented materials suggest that some major spectral features are not due to either texture or hydration but rather to the actual process of cementation. In particular, the anomalous strength of the restrahlen band in the $MgSO_4$ cemented mixtures compared to the $CaSO_4$ cemented mixtures cannot be explained by sample texture or hydration. The process of cementation must be different for the two types of sulfates. To examine what effects cementation had on these samples, we used elemental maps created with the electron microprobe to analyze the microscopic grain-to-grain relationships in the $MgSO_4$ and $CaSO_4$ cemented samples.

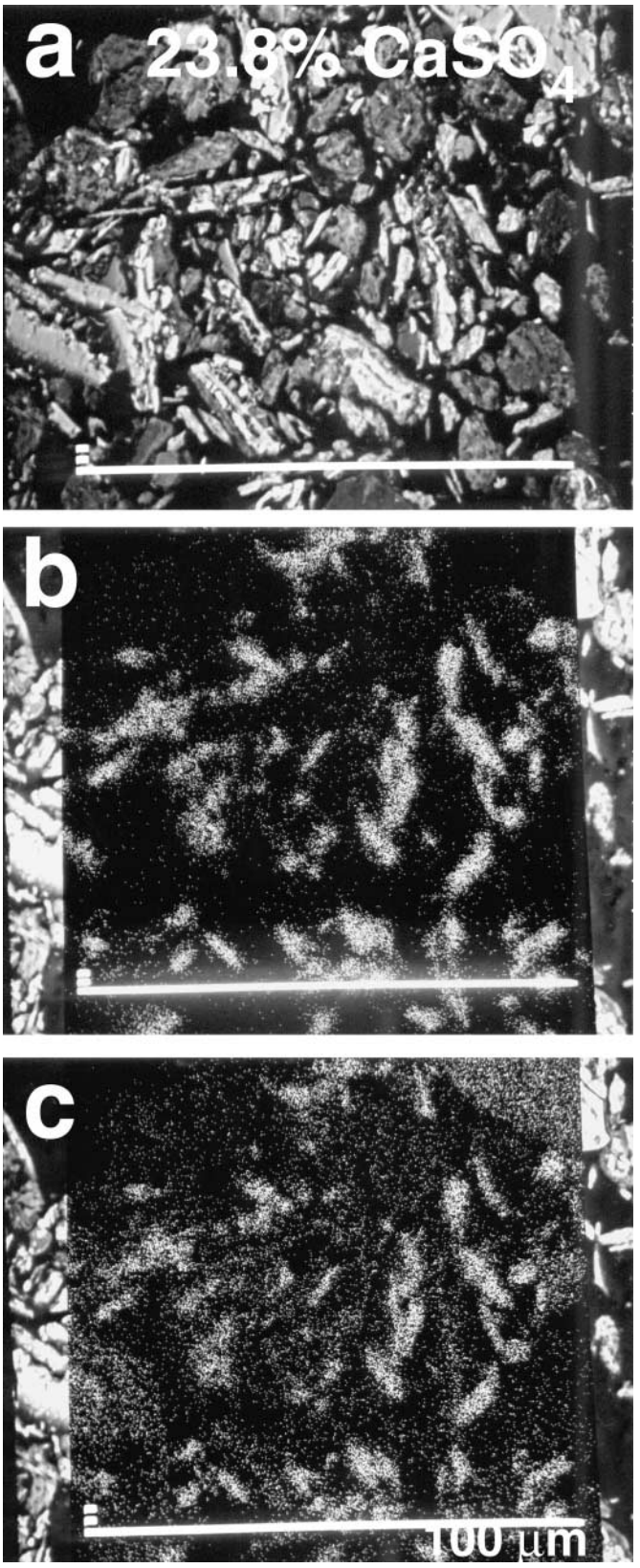

FIG. 8. Electron microprobe images of a thin section of cemented 23.8% $CaSO_4$ material. (a) Backscatter electron image; (b) sulfur elemental map; (c) calcium elemental map. The sulfate is mostly in discrete grains with only an extremely weak matrix compared to that in Fig. 9.

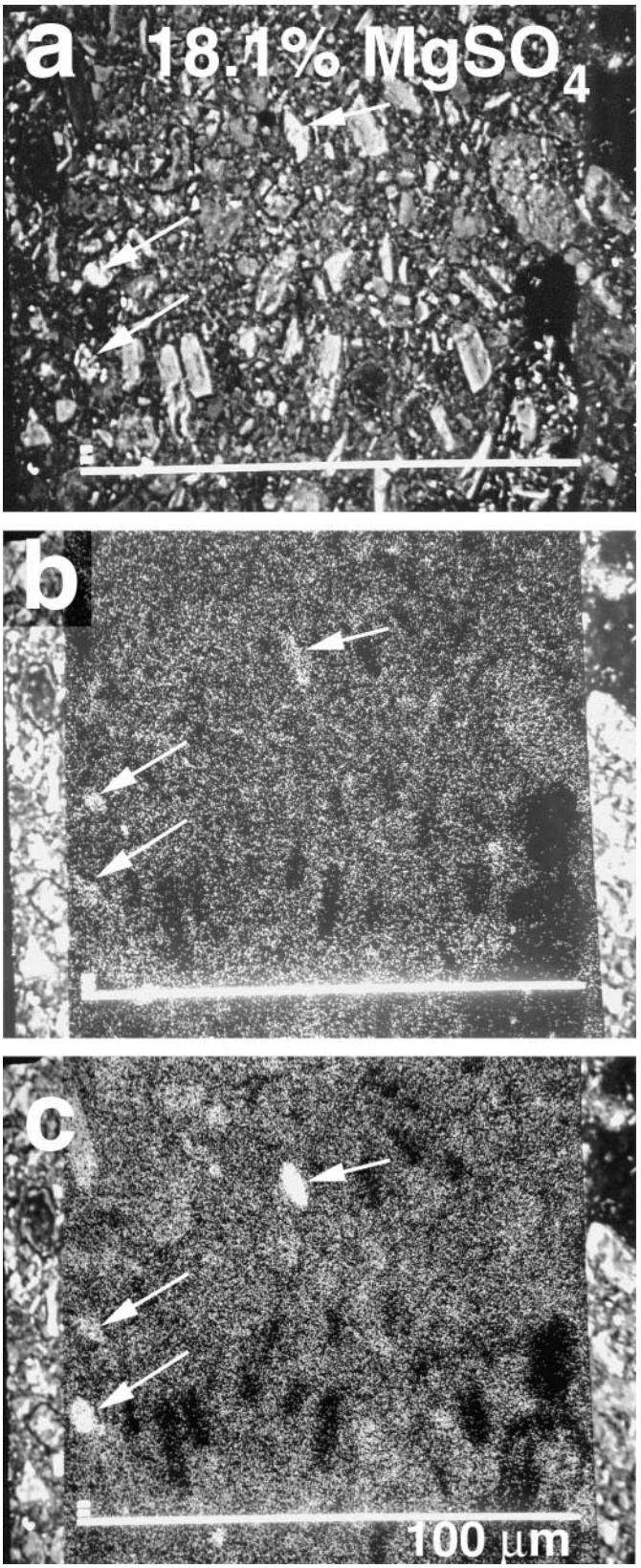

FIG. 9. Electron microprobe images of a thin section of cemented 18.1% $MgSO_4$ material. (a) Backscatter electron image; (b) sulfur elemental map; (c) magnesium elemental map. Arrows point out discrete grains of $MgSO_4$ in an otherwise diffuse matrix.

Electron backscatter results from the 23% $CaSO_4$ cemented mixture are shown in Fig. 8. The backscatter electron map (a) shows the locations of individual mineral grains. X-ray maps of the abundance of sulfur (b) and calcium (c) show that these elements are predominately located in individual grains. Here the sulfate does not form a diffuse matrix during the cementation process.

In contrast, the maps from the 18% $MgSO_4$ cemented mixture (Fig. 9) show that almost all of the sulfur (b) and magnesium (c) are dispersed in a matrix surrounding silicate grains. There are a few localized grains of $MgSO_4$ (arrows), but these comprise only a small portion of the view. $MgSO_4$ is much more soluble (260 g/L) in water than gypsum (2.4 g/L) at room temperature. It is likely that during cementation much of the relatively insoluble gypsum remained as discrete grains in the paste, while the extremely soluble $MgSO_4$ dissolved nearly completely and reprecipitated in a diffuse, encasing matrix. These differences would lead to the observed patterns of sulfate in the backscatter maps.

DISCUSSION

Together, the observations of sulfate–palagonite mixtures show that sulfates should be detectable in spectra of Mars depending on their physical nature and the wavelength range used for observation. Loose powders show relatively strong sulfate absorptions in the infrared between 4 and 5 μm but do not have strong features in the thermal infrared. When sulfate–palagonite mixtures are cemented a number of observable changes occur. The visible to near infrared is relatively unaffected, with only the shape of the 4–5 μm sulfate absorption changing in the $MgSO_4$ samples due to hydration of the sulfate. In the thermal infrared, the strength of the reflected continuum in cemented samples is due to increased compaction and decreased porosity of the material and not cementation explicitly. The most significant change in the spectra of cemented materials, and the change due solely to the cementation process, is the development of very strong sulfate restrahlen bands near 8.75 μm. On the basis of these experiments and spectral measurements, these features result from the actual process of cementation and not from packing. Differences in the solubility of $MgSO_4$ and $CaSO_4$ lead to differences in the microscopic structure of the laboratory cemented mixtures of these materials that translate to variations in the strength of the sulfate restrahlen bands. Understanding the nature of the spectra of mixtures of sulfates and neutral silicate materials and the factors affecting them has profound implications for the detection of sulfate minerals and interpretation of their textural and physical properties on Mars. Here we develop a model for the interaction of electromagnetic radiation with the cemented materials that explains the spectral and microphysical observations. Then we explore the impact that these observations have on studies of Mars.

Cementation Model

Based on the microscopic structure of the cemented materials and the associated spectral properties, we propose a model

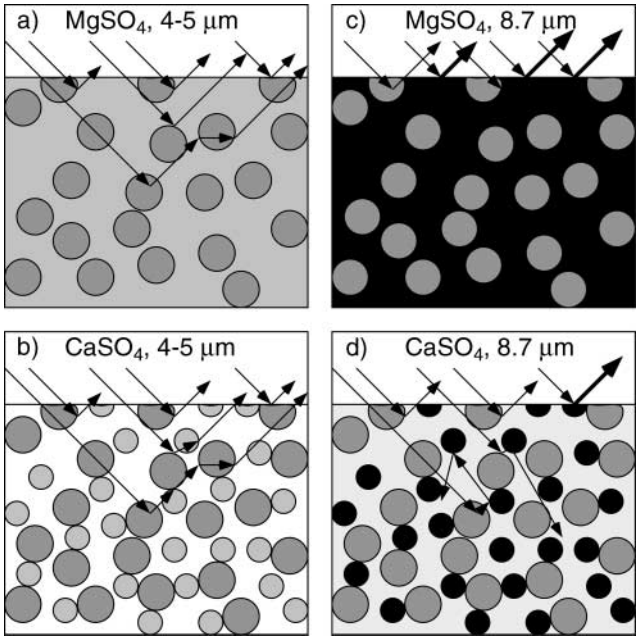

FIG. 10. Model of behavior of light interacting with cemented materials. (a) In the 4–5 μm range, $MgSO_4$ is relatively transparent (light gray matrix), and light is transmitted through while being absorbed in a way similar to a (near) particulate material such as the cemented $CaSO_4$ (b) where the sulfate is in small grains (light gray). (c) At the restrahlen wavelengths, the $MgSO_4$ is opaque (black), and light is only reflected off the first surface, in contrast with the particulate behavior of the cemented $CaSO_4$ (d) where light is able to penetrate the material because of the lack of a massive matrix. Bold arrows denote stronger reflections off of opaque, mirrorlike materials (depicted as black).

(Fig. 10) that explains the differences in spectral properties between the two types of cemented materials. This model describes the interaction of radiation with the sulfate mixtures and it can be concluded that the degree of reprecipitation and coating of the spectrally neutral palagonite by the various sulfate phases controls the strength of the 8.75-μm spectral feature. This feature is a reflectance peak caused by the high value of the absorption coefficient (the imaginary part of the complex index of refraction, k). The strength of this sulfate restrahlen band thus depends on the coherency of the sulfate surface because very little energy will pass through grain boundaries. Since the coherency of the sulfate surface is the key factor in controlling the magnitude of the restrahlen band, the physical size of particles is more important than the size of individual mineral grains (Cooper and Mustard 1999). Mineral grains that are clumped together appear as a single large particle to the incoming wavefront of light because the interaction with the solid surface depends on the spatial scale of the interface compared to the wavelength of light involved. This effect is even more critical when the value of k is high since the composite particle is then opaque to the incoming light.

The loose powder sulfate mixtures behave as a very fine particulate (Figs. 10a and 10b) with large amounts of diffuse surface scattering and an incoherent sulfate interface. This results in a lower reflectance for the restrahlen bands than would be observed for solid surfaces (Salisbury and Wald 1992, Salisbury *et al.* 1994, Mustard and Hays 1997, Cooper and Mustard 1999). When the sulfate–palagonite mixtures are cemented, they behave as a more massive material. In particular, when the sulfate phase has a spatial scale or coherence that is large relative to the wavelengths involved, it will scatter light coherently due to the mirrorlike k values (shown in black in Fig. 10c) and thus will have strong absorptions (reflection peaks) for the restrahlen bands. This is the case for the magnesium sulfate cemented materials. The reprecipitation of the sulfate around and between all of the silicate grains causes radiation to interact with it as a solid material of larger particle size. In contrast, the calcium sulfate cemented materials have had very little reprecipitation, and the sulfate exists as discrete grains dispersed among the silicate material (Fig. 10d). Radiation interacting with this mixture will see the separate sulfate grains and scatter off of them as if they were in a very fine particulate, with a relatively weak 8.75-μm restrahlen peak. Poorly cemented materials will therefore have weaker sulfate fundamentals in the thermal infrared than more homogeneously cemented mixtures.

In contrast, the absorptions between 4 and 5 μm have lower values of k. This means that radiation of these wavelengths will transmit through the sulfate phases relatively easily. The well-cemented materials still retain many surfaces inside the sulfate matrix because of the boundaries between the palagonite grains and the diffuse, very fine grained matrix. With the low value of k, the radiation penetrates the matrix and will undergo volume scattering off of the many internal boundaries (Fig. 10a). It will thus behave in a similar way to a particulate mixture or weakly cemented mixture with the same overall abundance of sulfate (Fig. 10b). In the loose mixture there are a large number of grain surfaces for multiple scattering, and this scattering will lead to roughly the same amount of transmission through sulfate grains as in the case of a well-cemented material. Thus the degree of cementation has little impact on the amount of transmission through sulfate in volume scattering regimes (spectral regions with low values of k) and will not change the strength of the weaker sulfate absorptions between 4 and 5 μm very much.

Implications for Mars

Because the visible to near-infrared and the thermal infrared portions of the sulfate mixture spectra respond quite differently to cementation, they provide complementary information about the material being observed. The features between 4 and 5 μm are relatively insensitive to the physical state of the material compared to the 8.75-μm restrahlen feature. At 8.75 μm, the strength of the reflectance peak depends on both the degree of cementation and the amount of sulfate in the mixture. The near-infrared absorptions between 4 and 5 μm are more sensitive to the total amount of sulfate in the mixtures and are relatively unaffected by the physical state of the material. This difference in behavior in the two wavelength regimes could be exploited to provide information about the total abundance and physical state of the sulfate mixtures. This analysis is demonstrated graphically

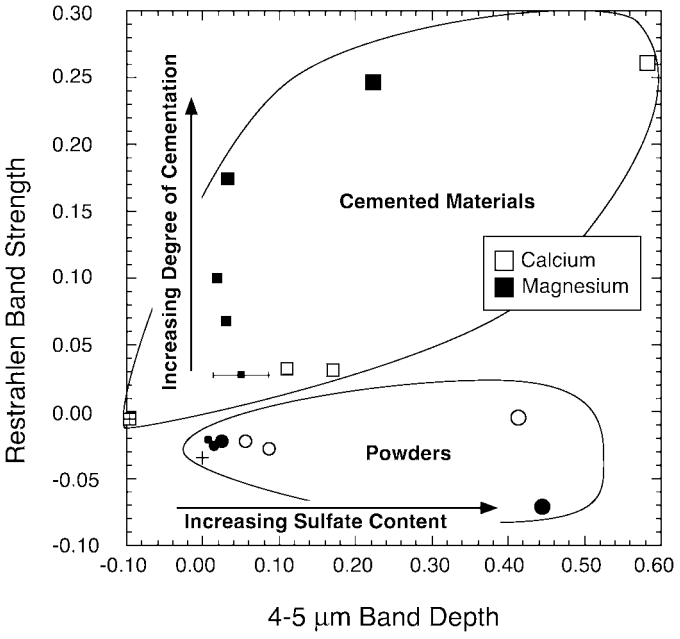

FIG. 11. Restrahlen band strength plotted against 4–5 μm band depth for all samples. Cemented materials are shown as squares, and loose powders as circles. These materials are easily separated in this parameter space. In cemented materials, the restrahlen band strength is affected by sulfate content and degree of cementation. The error bar shown is an estimate of the uncertainty in the 4–5 μm band depth due to varying degrees of hydration of the samples.

in Fig. 11. The restrahlen band strengths are plotted against the 4–5 μm band depths for all samples measured. The loose powders are distinguished from the cemented materials clearly. The cemented materials show a broader behavior. For a given sulfate content (4–5 μm band depth), the strength of the restrahlen band indicates whether the material is strongly or weakly cemented. Conversely, the strength of the 4–5 μm band indicates how much sulfate is in a material of given restrahlen band strength. Large 4–5 μm band depths indicate large amounts of weakly cemented sulfate, while small band depths indicate a strongly cemented, lower sulfate matrix. Therefore, the inclusion of the 4–5 μm band information with the restrahlen band strengths allows both sulfate content and physical state to be estimated.

The laboratory samples used in this study are good spectral analogs for sulfate-bearing soils on Mars. Loose powders match the bulk composition and physical state of loose surface fines while the cemented samples have physical and chemical properties analogous to those of the indurated materials seen at the Viking Lander sites. The laboratory samples do not differentiate among the likely cations associated with the sulfate *per se*. The restrahlen band strength depends on the degree of cementation, which is controlled by the amount of dissolution and reprecipitation in the form of a diffuse matrix. Either magnesium or calcium could form a well-cemented crust (especially with low pH, large amounts of water, and long time scales), but for any given set of conditions, magnesium sulfate is more soluble.

The differences in the behavior of loose powders and cemented mixtures of sulfates and silicates in the wavelength regimes discussed here imply that well-cemented soils with a diffuse sulfate matrix (whether calcium or magnesium in composition) will be much easier to detect in thermal infrared spectra of Mars. Conversely, areas covered by loose dust will appear spectrally bland regardless of the composition of underlying material. An interesting question then is whether cemented material that has been disaggregated by erosion would appear as a crust or as a powder in terms of the strength of the restrahlen band. One magnesium sulfate crust was crushed and sieved to particle sizes of 500–1000 μm. Its spectrum, shown in Fig. 7a, clearly demonstrates that the restrahlen band completely disappears. This means that disaggregated crusts will lose their distinguishing spectroscopic feature because the microscopic coherency of the sulfate cement is lost on the rough surfaces of these sand-sized particles.

In terms of detecting cemented sulfate-bearing soils on Mars, the areal abundance of the material will be critical. Because spectroscopic remote sensing techniques only sample the upper 100 μm of a surface, even thin layers of atmospherically deposited dust can obscure the spectral characteristics of a surface material such as cemented sulfates, making it difficult to compare inferred compositions with Viking XRF measurements of excavated samples. The improved spatial resolutions offered now by TES and later by THEMIS allow these instruments to capture more information about smaller areas that are unobscured by dust than was possible with earlier instruments with poorer spatial resolution. This will enhance their ability to detect small patches of exposed sulfate-cemented soils.

To investigate the effect of obscuration by dust and to estimate its impact in a quantitative manner, we mathematically created linear mixtures of sulfate–palagonite dust spectra and cemented soil spectra (Fig. 12). The spectrum of the powder

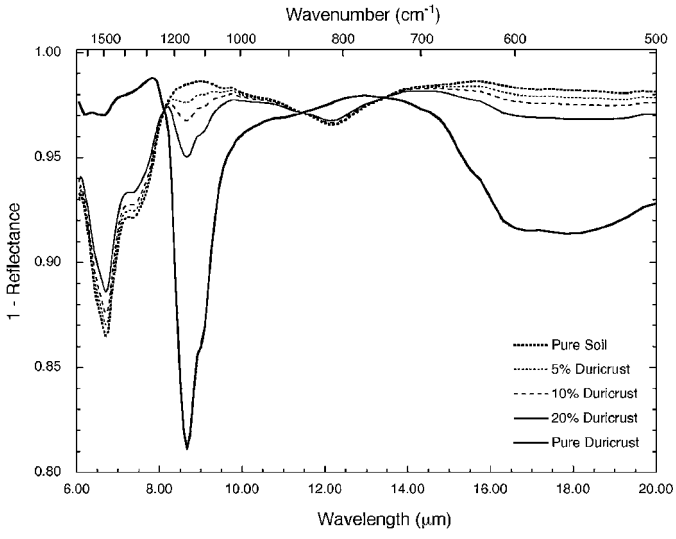

FIG. 12. Simulated emission spectra of duricrust on Mars that is partially obscured by sulfate-bearing dust. Spectra are calculated from mathematical mixtures of cemented and loose $MgSO_4$ materials and inverted to apparent emissivity using Kirchhoff's Law. The restrahlen band at 8.75 μm is detectable if 5–10% of the surface area is exposed duricrust.

mixture that most closely matches the sulfate content of loose fines (10% $MgSO_4$) is used to simulate the obscuring dust. It is combined with varying proportions of the spectrum of the cemented mixture that is closest in composition to the crusty to cloddy soils (12.4% $MgSO_4$) seen at the Viking landing sites. The spectra were convolved to TES resolution before being linearly mixed, and the result was converted to apparent emissivity using Kirchhoff's law. The 8.75-μm restrahlen band indicative of the cemented material becomes difficult to detect when the cemented material makes up less than $\sim$10% of the composite spectrum. This indicates that for detecting sulfate-cemented soils on Mars using TES, at least 10% of the area of a pixel must contain dust-free sulfate-cemented soils. The higher spatial resolution provided by THEMIS should therefore allow correspondingly smaller patches of cemented materials to be detected. High-resolution near-infrared data by OMEGA should allow the actual sulfate content of such areas to be determined. There are two complications for the OMEGA observations in the 4–5 μm region for sulfate studies of Mars. First, the presence of a saturated atmospheric CO_2 absorption between 4.2 and 4.4 μm superimposes on the sulfate absorptions. Second, the radiance from the surface consists of subequal amounts of reflected solar irradiance and emitted thermal radiance. Nevertheless, combining 4–5 μm observations with thermal infrared data will then constrain the degree of cementation of the material.

CONCLUSIONS

The laboratory samples created in this study are good analogs to investigate the effects of sulfate cementation on spectral properties of mixtures of materials that are representative of those on Mars. The presence of indurated soils on Mars provides a source of information on the past climate of the planet and processes active in the low-water environment that exists today. While the method of preparation of these samples is not an analog for the processes that have created indurated soils on Mars, these materials provide important information for use in interpreting remotely sensed spectra in the context of understanding sulfate-bearing soils.

Sulfate spectral features in the 4–5 and 8–9 μm ranges provide complementary information about the composition, abundance, and physical state of sulfate in mixtures. The 4–5 μm range is relatively insensitive to the physical state of the mixture and provides information on the sulfate content for both loose powder and cemented mixtures. In contrast, the sulfate fundamental at 8.75 μm is very sensitive to the degree of cementation. Mixtures that are strongly cemented where the sulfate is in a diffuse, pervasive matrix surrounding all of the silicate components of the palagonite exhibit a very strong restrahlen band due to the sulfate vibrational fundamental. This comes from the coherent, mirrorlike surface of the homogeneous sulfate matrix in the high-absorption-coefficient spectral regions. In contrast, poorly cemented mixtures have sulfate that remains in discrete grains that multiply scatter light in a manner akin to a loose particulate. This leads to a weaker 8.75-μm feature because multiple scatters off of high-absorption-coefficient material result in less reflectance.

The unique behavior of the two sets of sulfate features means that together they can be used to determine the abundance and physical state of sulfate on the martian surface. TES observations have the chance to detect sulfate-cemented soils on Mars provided that 10% of a pixel consists of dust-free cemented soils. Future observations by a spectrometer capable of collecting data in the 4–5 μm range (such as OMEGA) will be able to provide information on the sulfate content of all soils regardless of their texture. Combined with information from TES or THEMIS, this will allow characterization of both the degree of cementation and the sulfur content of surface materials on Mars.

ACKNOWLEDGMENTS

We thank T. Hiroi for measuring samples in RELAB and J. Devine for operating the electron microprobe. We also thank S. Murchie and D. Blaney for helpful reviews of this manuscript. We are grateful to NASA and the Keck Foundation for RELAB facilities support and to the Keck Foundation for microprobe facility support. This paper is based upon work supported under a NSF Graduate Fellowship and by NASA under Grant NAG5-4162.

REFERENCES

Adams, J. B. 1975. Interpretation of visible and near-infrared diffuse reflectance spectra of pyroxenes and other rock-forming minerals. In *Infrared and Raman Spectroscopy of Lunar and Terrestrial Minerals* (C. Karr, Ed.), pp. 94–116. Academic Press, New York.

Allen, C. C., J. L. Gooding, M. Jercinovic, and K. Keil 1981. Altered basaltic glass: A terrestrial analog to the soil of Mars. *Icarus* **45**, 347–369.

Allen, C. C., R. V. Morris, K. M. Jager, D. C. Golden, D. J. Lindstrom, M. M. Lindstrom, and J. P. Lockwood 1998. Martian regolith simulant JSC Mars-1. *Lunar Planet. Sci.* **29**, 1690 (abstract).

Baird, A. K., A. J. Castro, B. C. Clark, I. P. Toulmin, J. H. Rose, K. Keil, and J. Gooding 1977. The Viking X-ray fluorescence experiment: Sampling strategies and laboratory simulations. *J. Geophys. Res.* **82**, 4595–4624.

Bandfield, J. L., V. E. Hamilton, and P. R. Christensen 2000. A global view of martian surface compositions from MGS-TES. *Science* **287**, 1626–1630.

Banin, A., T. Ben-Shlomo, L. Margulies, D. F. Blake, R. L. Mancinelli, and A. U. Gehring 1993. The nanophase iron mineral(s) in Mars soil. *J. Geophys. Res.* **98**, 20831–20853.

Banin, A., F. X. Han, I. Kan, and A. Cicelsky 1997. Acidic volatiles and the Mars soil. *J. Geophys. Res.* **102**, 13341–13356.

Bell, J. F., T. B. McCord, and P. D. Owensby 1990. Observational evidence of crystalline iron oxides on Mars. *J. Geophys. Res.* **95**, 14447–14461.

Bell, J. F., R. V. Morris, and J. B. Adams 1993. Thermally altered palagonitic tephra: A spectral and process analog to the soil and dust of Mars. *J. Geophys. Res.* **98**, 3373–3385.

Bell, J. F., H. Y. McSween Jr., J. A. Crisp, R. V. Morris, S. L. Murchie, N. T. Bridges, J. R. Johnson, D. R. Britt, M. P. Golombek, H. J. Moore, A. Ghosh, J. L. Bishop, R. C. Anderson, J. Brückner, T. Economou, J. P. Greenwood, H. P. Gunnlaugsson, R. M. Hargraves, S. Hviid, J. M. Knudsen, M. B. Madsen, R. Reid, R. Rieder, and L. Soderblom 2000. Mineralogic and compositional properties of martian soil and dust: Results from Mars Pathfinder. *J. Geophys. Res.* **105**, 1721–1755.

Binder, A. B., R. E. Arvidson, E. A. Guinness, K. L. Jones, E. C. Morris, T. A. Mutch, D. C. Pieri, and C. Sagan 1977. The geology of the Viking Lander 1 site. *J. Geophys. Res.* **82**, 4439–4451.

Bishop, J. L., C. M. Pieters, and R. G. Burns 1993. Reflectance and Mössbauer spectroscopy of ferrihydrite-montmorillonite assemblages as Mars soil analog materials. *Geochim. Cosmochim. Acta* **57**, 4583–4595.

Blaney, D. L., and T. B. McCord 1995. Indications of sulfate minerals in the martian soil from Earth-based spectroscopy. *J. Geophys. Res.* **100**, 14433–14441.

Burns, R. G. 1993. Rates and mechanisms of chemical weathering of ferromagnesian silicate minerals on Mars. *Geochim. Cosmochim. Acta* **57**, 4555–4574.

Catling, D. C. 1999. A chemical model for evaporites on early Mars: Possible sedimentary tracers of the early climate and implications for exploration. *J. Geophys. Res.* **104**, 16453–16469.

Christensen, P. R., J. L. Bandfield, R. N. Clark, K. S. Edgett, V. E. Hamilton, T. Hoefen, H. H. Kieffer, R. O. Kuzmin, M. D. Lane, M. C. Malin, R. V. Morris, J. C. Pearl, R. Pearson, T. L. Roush, S. W. Ruff, and M. D. Smith 2000a. Detection of crystalline hematite mineralization on Mars by the Thermal Emission Spectrometer: Evidence for near-surface water. *J. Geophys. Res.* **105**, 9623–9642.

Christensen, P. R., J. L. Bandfield, M. D. Smith, V. E. Hamilton, and R. N. Clark 2000b. Identification of a basaltic component on the martian surface from Thermal Emission Spectrometer data. *J. Geophys. Res.* **105**, 9609–9621.

Clark, B. C. 1993. Geochemical components in martian soil. *Geochim. Cosmochim. Acta* **57**, 4575–4581.

Clark, B. C., and A. K. Baird 1979. Volatiles in the martian regolith. *Geophys. Res. Lett.* **6**, 811–814.

Clark, B. C., and D. C. V. Hart 1981. The salts of Mars. *Icarus* **45**, 370–378.

Clark, B. C., A. K. Baird, R. J. Weldon, D. M. Tsusaki, L. Schnabel, and M. P. Candelaria 1982. Chemical composition of martian fines. *J. Geophys. Res.* **87**, 10059–10067.

Clark, R. N. 1999. Spectroscopy and principles of spectroscopy. In *Manual of Remote Sensing* (A. N. Rencz, Ed.), pp. 3–58. Wiley, New York.

Clark, R. N., and T. L. Roush 1984. Reflectance spectroscopy: Quantitative analysis techniques for remote sensing applications. *J. Geophys. Res.* **89**, 6329–6340.

Cooper, C. D., and J. F. Mustard 1999. Effects of very fine particle size on reflectance spectra of smectite and palagonitic soil. *Icarus* **142**, 557–570.

Crown, D. A., and C. M. Pieters 1987. Spectral properties of plagioclase and pyroxene mixtures and the interpretation of lunar soil spectra. *Icarus* **72**, 492–506.

Erard, S., J. Mustard, S. Murchie, and J.-P. Bibring 1994. Martian aerosols: Near-infrared spectral properties and effects on the observation of the surface. *Icarus* **111**, 317–337.

Ferguson, D. C., J. C. Kokecki, M. W. Siebert, D. M. Wilt, and J. R. Matijevic 1999. Evidence for martian electrostatic charging and abrasive wheel wear from the Wheel Abrasion Experiment on the Pathfinder Sojourner rover. *J. Geophys. Res.* **104**, 8747–8760.

Griffith, L. L., and E. L. Shock 1997. Hydrothermal hydration of martian crust: Illustration via geochemical model calculations. *J. Geophys. Res.* **102**, 9135–9143.

Hapke, B. 1983. *Theory of Reflectance and Emittance Spectroscopy.* Cambridge Univ. Press, Cambridge, UK.

Hunt, G. R., and R. K. Vincent 1968. The behavior of spectral features in the infrared emission from particulate surfaces of various grain sizes. *J. Geophys. Res.* **73**, 6039–6046.

Johnson, J. R., P. G. Lucey, K. A. Horton, and E. M. Winter 1998. Infrared measurements of pristine and disturbed soils 1. Spectral contrast differences between field and laboratory data. *Remote Sensing Environ.* **64**, 34–46.

Lane, M. D., and P. R. Christensen 1998. Thermal infrared emission spectroscopy of salt minerals predicted for Mars. *Icarus* **135**, 528–536.

Lyon, R. J. P. 1964. *Evaluation of Infrared Spectraphotometry for Compositional Analysis of Lunar and Planetary Soils, Part II, Rough and Powdered Surfaces.* NASA Report CR-100.

Lyon, R. J. P. 1965. Analysis of rocks by spectral infrared emission (8 to 25 microns). *Econ. Geol.* **60**, 717–736.

McSween, H. Y., and K. Keil 2000. Mixing relationships in the martian regolith and the composition of globally homogeneous dust. *Geochim. Cosmochim. Acta* **64**, 2155–2166.

Moersch, J. E., and P. R. Christensen 1995. Thermal emission from particulate surfaces: A comparison of scattering models with measured spectra. *J. Geophys. Res.* **100**, 7465–7477.

Moore, H. J., R. M. Hutton, G. D. Clow, and C. R. Spitzer 1987. *Physical Properties of the Surface Materials at the Viking Landing Sites on Mars.* U.S.G.S. Professional Paper 1389.

Moore, H. J., D. B. Bickler, J. A. Crisp, H. J. Eisen, J. A. Gensler, A. F. C. Haldemann, J. R. Matijevic, L. K. Reid, and F. Pavlics 1999. Soil-like deposits observed by Sojourner, the Pathfinder rover. *J. Geophys. Res.* **104**, 8729–8746.

Moore, J. M., and M. A. Bullock 1999. Experimental studies of Mars-analog brines. *J. Geophys. Res.* **104**, 21925–21934.

Morris, R. V., D. G. Agresti, J. H. V. Lauer, J. A. Newcomb, T. D. Shelfer, and A. V. Murali 1989. Evidence for pigmentary hematite on Mars based on optical, magnetic, and Mössbauer studies of superparamagnetic (nanocrystalline) hematite. *J. Geophys. Res.* **94**, 2760–2778.

Morris, R. V., D. C. Golden, J. F. Bell III, J. H. V. Lauer, and J. B. Adams 1993. Pigmenting agents in martian soils: Inferences from spectral, Mössbauer, and magnetic properties of nanophase and other iron oxides in Hawaiian palagonitic soil PN-9. *Geochim. Cosmochim. Acta* **57**, 4597–4609.

Morris, R. V., D. C. Golden, J. F. Bell III, T. D. Shelfer, A. C. Scheinost, N. W. Hinman, G. Furniss, S. A. Mertzman, J. L. Bishop, D. W. Ming, C. C. Allen, and D. T. Britt 2000. Mineralogy, composition, and alteration of Mars Pathfinder rocks and soils: Evidence from multispectral, elemental, and magnetic data on terrestrial analogue, SNC meteorite, and Pathfinder samples. *J. Geophys. Res.* **105**, 1757–1817.

Murchie, S., J. F. Mustard, S. Erard, J. L. Bishop, J. W. Head, and C. M. Pieters 1993. Spatial variation in the spectral properties of bright regions on Mars. *Icarus* **105**, 454–468.

Mustard, J. F. 1997. Chemical and mineralogical processes in martian soil. In *Conference on Early Mars: Geologic and Hydrologic Evolution, Physical and Chemical Environments, and the Implications for Life* (S. M. Clifford, A. H. Treimar, H. E. Newsom, and J. D. Farmer, Eds.), pp. 59–60. LPI Contrib. No. 916, Lunar and Planetary Institute, Houston.

Mustard, J. F., and J. E. Hays 1997. Effects of hyperfine particles on reflectance spectra from 0.3 to 25 μm. *Icarus* **125**, 145–163.

Mustard, J. F., and C. M. Pieters 1989. Photometric phase functions of common geologic minerals and applications to quantitative analysis of mineral mixture reflectance spectra. *J. Geophys. Res.* **94**, 13619–13634.

Mustard, J. F., and J. M. Sunshine 1995. Seeing through the dust: Martian crustal heterogeneity and links to the SNC meteorites. *Science* **267**, 1623–1626.

Newsom, H. E., J. J. Hagerty, and F. Groff 1999. Mixed hydrothermal fluids and the origin of the martian soil: A new quantitative model. *Lunar Planet. Sci.* **30**, 1262 (abstract).

Pieters, C. M. 1983. Strength of mineral absorption features in the transmitted component of near-infrared reflected light: First results from RELAB. *J. Geophys. Res.* **88**, 9534–9544.

Pollack, J. B., T. Roush, F. Witteborn, J. Bregman, D. Wooden, C. Stoker, O. B. Toon, D. Rank, B. Dalton, and R. Freedman 1990. Thermal emission spectra of Mars (5.4–10.5 μm): Evidence for sulfates, carbonates, and hydrates. *J. Geophys. Res.* **95**, 14595–14627.

Pollack, J. B., M. E. Ockert-Bell, and M. K. Shepard 1995. Viking Lander image analysis of martian atmospheric dust. *J. Geophys. Res.* **100**, 5235–5250.

Rieder, R., T. Economou, H. Wänke, A. Turkevich, J. Crisp, J. Brückner, G. Dreibus, and J. H. Y. McSween 1997. The chemical composition of martian soil and rocks returned by the Mobile Alpha Proton X-ray Spectrometer: Preliminary results from X-ray mode. *Science* **278**, 1771–1774.

Salisbury, J. W., and J. W. Eastes 1985. The effect of particle size and porosity on spectral contrast in the mid-infrared. *Icarus* **64**, 586–588.

Salisbury, J. W., and A. Wald 1992. The role of volume scattering in reducing spectral contrast of reststrahlen bands in spectra of powdered minerals. *Icarus* **96**, 121–128.

Salisbury, J. W., L. S. Walter, N. Vergo, and D. M. D'Aria 1991. *Infrared (2.1–25 μm) Spectra of Minerals*. Johns Hopkins Univ. Press, Baltimore.

Salisbury, J. W., A. Wald, and D. M. D'Aria 1994. Thermal-infrared remote sensing and Kirchhoff's law 1. Laboratory measurements. *J. Geophys. Res.* **99**, 11897–11911.

Schaefer, M. W. 1993. Aqueous geochemistry on early Mars. *Geochim. Cosmochim. Acta* **57**, 4619–4625.

Settle, M. 1979. Formation and deposition of volcanic sulfate aerosols on Mars. *J. Geophys. Res.* **84**, 8343–8354.

Singer, R. B., T. B. McCord, and R. N. Clark 1979. Mars surface composition from reflectance spectroscopy: A summary. *J. Geophys. Res.* **84**(B14), 8415–8426.

Tomasko, M. G., L. R. Doose, M. Lemmon, P. Smith, and E. Wegryn 1999. Properties of dust in the martian atmosphere from the imager for Mars Pathfinder. *J. Geophys. Res.* **104**, 8987–9008.

Toulmin, P., A. K. Baird, B. C. Clark, K. Keil, J. H. J. Rose, R. P. Christian, P. H. Evans, and W. C. Kelliher 1977. Geochemical and mineralogical interpretation of the Viking inorganic chemical results. *J. Geophys. Res.* **84**, 4625–4634.

Vincent, R. K., and G. R. Hunt 1968. Infrared reflectance from mat surfaces. *Appl. Opt.* **7**, 53–58.